2014 IEEE/RSJ International Conference on
Intelligent Robots and Systems (IROS 2014)
September 14-18, 2014, Chicago, IL, USA

Automatic Detection and Verification of Pipeline Construction Features with Multi-modal data

Teresa Vidal-Calleja[1], Jaime Valls Miró[1], Fernando Martín[2], Daniel C. Lingnau[3] and David E. Russell[3]

***Abstract*— Assessment of the condition of underground pipelines is crucial to avoid breakages. Autonomous in-line inspection tools provided with Non-destructive Technology (NDT) sensors to assess large sections of the pipeline are commonly used for these purposes. An example of such sensors based on Eddy currents is the Remote Field Technology (RFT). A crucial step during in-line inspections is the detection of construction features, such as joints and elbows, to accurately locate and size specific defects within pipe sections. This step is often performed manually with the aid of visual data, which results in slow data processing. In this paper, we propose a generic framework to automate the detection and verification of these construction features using both NDT sensor data and visual images. Firstly, supervised learning is used to identify the construction features in the NDT sensor signals. Then, image processing is employed to verify the selection. Results are presented with data from a RFT tool, for which a specialised descriptor has been designed to characterise and classify its signal features. Furthermore, the construction feature is displayed in the image, once it is identified in the RFT data and detected in the visual data. A visual odometry algorithm has been implemented to locate the visual data with respect to the RFT data. About 800 meters of these multi-modal data are evaluated to test the validity of the proposed approach.**

I. INTRODUCTION

Deterioration of pipelines used in water, oil and gas transportation systems can lead to leaks and breakages that can result in significant damages, expensive repair costs and cause major inconvenience to the public. Detailed inspection of this critical infrastructure to monitor for corrosion and general pipeline wall thickness reduction is therefore a top priority for utilities.

In current industry practice, direct inspection is generally performed using Non-Destructive Testing (NDT) sensors. Some are located external to the pipe to assess a localised area, others are inserted by means of an in-line tool to inspect larger sections of the network in one go. Examples of NDT sensing techniques include acoustics that measure time-of-flight [1], Magnetic Flux Leakage (MFL) that measure variations of signal amplitude in magnetic fields [2], and remote field Eddy current that measure both time-of-flight and signal strength of a varying electromagnetic field [3].

The remote field Eddy current technique, also known as Remote Field Technology (RFT) has the capability of measuring the wall thickness of ferromagnetic pipes, as well as detecting and sizing flaws therein. This technology is commonly employed in in-line tools, such as the autonomous RFT inspection tool shown in Fig. 1(a).

(a) RFT tool (b) CCTV tool

Fig. 1. Inspection platforms that travel inside pipes. a) Russell NDE Systems Inc. See-Snake in-line tool used to detect pipeline corrosion, pitting, wall thinning and graphitisation. b) Wheeled mobile robot equipped with a single camera used to visually inspect pipelines.

Autonomous, in-line tools have the great advantage of inspecting large sections of a pipeline in relatively short time (4-5 h/km). Locating such tools within the pipeline, however, is a real challenge. The main issue is that these tools are commonly driven by the water flow and the primary sensors used for localisation purposes are wheel encoders[1]. In order to overcome the unreliability of the encoders, a verification step through the identification of construction features (e.g. joints, elbows) is essential to be able to accurately locate the tool and associated measurements within the pipe sections (between joints). CCTV (Closed Circuit TV) inspections (see Fig. 1(b)) are useful in this process, where visual images of the empty pipeline are stored for further analysis. Construction features in this kind of images are detectable for the expert eye. Because this verification process is, in general, performed manually by an analyst, results are increasingly time consuming.

This paper aims to automate the verification process through Construction Features (CF) identification and video verification using NDT sensor signals (*e.g.* RFT) and visual images. Three main contributions are presented in this manuscript; 1) A framework to automatically verify CF for in-line inspections with NDT sensors, 2) a specialised descriptor of the RFT sensor signals for CF identification and 3) a circle-like feature detection in visual images of potential CF for automatic verification.

The identification process of the CF is set as a classification problem on the sensor signals based on supervised learning. We propose an approach to detect the pipeline

[1]T. Vidal-Calleja and J. Valls Miró are with the Centre of Autonomous Systems, Faculty of Engineering and IT, University of Technology, Sydney NSW 2007, Australia. Teresa.VidalCalleja@uts.edu.au and Jaime.VallsMiro@uts.edu.au

[2]F. Martín is with Systems Engineering and Automation, Carlos III University, Madrid, Spain. fmmonar@ing.uc3m.es

[3]D. C. Lingnau and D. E. Russell are with Russell NDE Systems Inc, Alberta, Canada. dlingnau@russelltech.com and drussell@russelltech.com

[1]Low visibility conditions such as darkness or turbid waters preclude the direct use of some type of extereoceptive sensors.

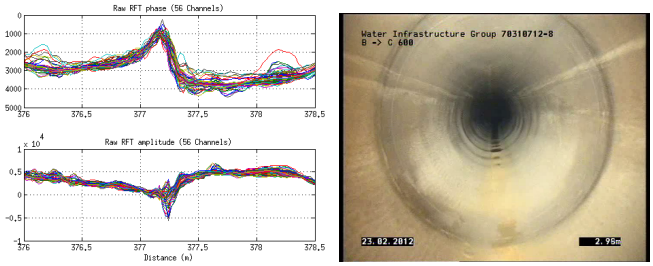

(a) RFT data (b) CCTV data

Fig. 2. Examples of a B&S joint on multi-modal data. a) Shows the phase and amplitude for the 56 channels of the RFT sensing tool around the B&S joint located at 377.2m. b) Shows the visual image at 1m behind the location of the B&S.

CF such as joints, flanges and elbows through the use of Support Vector Machines (SVM) [4]. The algorithm relies on a new feature descriptor for RFT signals that incorporates the Hjorth parameters [5]. The output of the classifier is the CF axial position within the pipe, which is handed over to the verification process.

Recent work on signal processing and classification with magnetic sensor data used in inspection applications can be found in the literature. For instance, in [6] MFL sensors are employed to detect defects and anomalies in oil and gas pipelines. Also for MFL sensors our work [7] on multiple defect characterisation with Gaussian process models. More specific for RFT signals, the work in [8] addressed defect characterisation using principal component analysis in simulated data. All these works are focused on the signal analysis for defect recognition, the work presented in here, however, is towards aiding the current practise to verify the location of the in-line tools. Closer to our work, regarding CF classification, is the one presented by [9], where Eddy current signals are employed to localise trains in topological maps with rail turnout identification.

Our complete framework, on the other hand, not only relies on classifying the NDT sensor data, but also on the use of processed images to automatically verify the identified CF. Colour difference (Delta E) on the LAB space [10] is used to extract the circle-like construction features in visual images. The proposed approach correctly verifies the CF that has been identified in the NDT sensor data and detected in the CCTV data at the same location. In order to automatically associate the location of the image with respect to the RFT data, a dedicated visual odometry algorithm has been implemented getting an estimate of the axial position of each image on the video sequence. The final output of our approach is the verified CF highlighted on the visual image corresponding to the position given by the classifier.

Actual data from a condition assessment inspection with the See-Snake RFT tool (Fig. 1(a)) and an independent CCTV inspection of the empty pipeline are used to evaluate the results of the proposed approach. An example of a typical CF, in this case a Bell & Spigot (B&S) joint, in both RFT data and a visual image is shown in Fig. 2. Approximately 800m of data have been evaluated on a 660mm diameter cast-iron water pipe. Ground-truth has been manually obtained by analysts from Russell NDE Systems Inc.

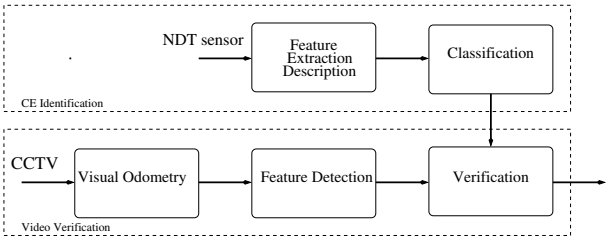

Fig. 3. Diagram of the framework for automatic detection and verification of pipeline construction features.

II. Generic Framework

The proposed approach aims to detect, identify and verify construction features found while inspecting the condition of underground pipelines. To do so it classifies features extracted from the signals of a NDT sensor based on Support Vector Machines [4]. In parallel, it detects high-contrast circle-like features commonly seen in visual images from empty pipelines using a similar approach to the proposed in [11] for 3D images. As we will discuss later, CF always appear as circle-like features in visual images, although not all of these features are CF. The output of the framework is the verification of the CF when both sources of multi-modal data are matched using its location.

Two main processes are the core of the framework:

- identification with NDT sensor data, and
- video verification.

Fig. 3 shows a diagram of the framework. Firstly, due to the high dimensionality of the data, features on the NDT sensor are extracted and characterised using a dedicated descriptor. Then, the classifier provides the position of the CF according to the sensor data. Independently, circle-like visual features are detected in the images. Finally, the identified CF is matched with the detected CF in the corresponding image sequence, based on the position provided by a visual odometry algorithm that locates the each image with respect to the reference frame provided by the NDT sensor tool.

The following two sections describe in detail the two main processes of the framework.

III. CF Identification applied to RFT sensor

The framework described in the previous section is particularised to be used with RFT data. Locally referenced phase and amplitude values of the RFT data along the pipeline are the raw signals to be processed in order to identify CF.

A. Remote Field Eddy Current

The RFT is an Eddy current pipe inspection technique [3]. A probe, that consists of an exciter coil and one or more detectors at an axial distance over two diameters from the exciter (termed the remote field), is moved through a conductive pipe. The exciter coil is driven with relatively low frequency sinusoidal current producing a magnetic field. The exciter field induces strong Eddy currents in the inner walls of the pipe near the exciter. These currents produce their own magnetic fields, which are always in opposition to the exciter

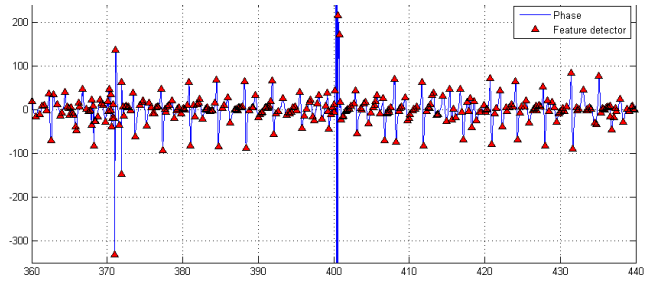

Fig. 4. Typical features produced by the peak and valley detector applied to $\hat{\alpha}(x)$.

field. Because Eddy currents experience conductive losses in the pipe walls, these counter fields do not equally balance the exciting field. Construction features and anomalies are thus detectable because they interfere with the preferred Eddy current paths and magnetic fields.

RFT tools measure the "time of flight" (phase shift) and the signal strength (amplitude) of a signal emitted by an exciter coil and detected by an array of receivers. In the tool used for this work (Fig. 1(a)), the receivers are positioned circumferentially. 56 channels give the phase and amplitude around the pipe. For each cycle of the exciter frequency, a clock is started and the arrival time of the signal at the detector is used to reset the clock. The time interval gives a measurement of the time of flight.

Odometry readings are integrated with the signal reading to be associated directly with the location of the pipe from where they were taken. Phase and log-amplitude are the preferred readings because they are both linear indicators of overall wall thickness. Fig. 2(a) presents an example of the phase and amplitude readings with respect to its axial position. As figure shows the RFT signals change in the presence of CF such as B&S joints.

B. Detectors and Descriptors

Signal feature extraction (also known as feature detection) is a well-known mechanism use to map sensor signals into a lower dimensional space. For feature extraction, we propose to use a peak and valley detector on the normalised RFT phase signal

$$\hat{\alpha}(x) = \sum_{j=1}^{n} \mathtt{SMA} \frac{\alpha^j(x) - \overline{\alpha^j(x)}}{\sigma_\alpha^j}, \tag{1}$$

where SMA is the simple moving average, x is the axial position, and α^j is the phase of the jth channel with $\overline{\alpha^j}$ and σ_α^j as the mean and standard deviation respectively. The ith peak or valley is given by x_{P_i}. An example of these features (between the axial location from 360m to 440m) is presented in Fig. 4.

Multiple basic characteristics of the peaks and valleys are concatenated to generate the feature descriptor. The proposed feature descriptor for RFT signals is given by

$$\mathbf{x}_i = [\hat{\alpha}(x_{P_i}), \hat{a}(x_{P_i}), \hat{da}(x_{P_i}), A_i, M_i, C_i], \tag{2}$$

where $\hat{\alpha}(x_P)$ is the phase magnitude of the peak or valley, $\hat{a}(x_P)$ is the amplitude value at peak or valley location, $\hat{da}(x_P)$ the derivative of the amplitude and, more importantly, the A, M and C are Hjorth parameters [5] of a window surrounding the peak.

Hjorth parameters has predominantly been used in electroencephalography (EEG) signal description. These parameters are also known as the normalised slope descriptors and are defined as follows;

- activity: $A = \sigma_\alpha^2$,
- mobility: $M = \sigma_{d\alpha}/\sigma_\alpha$
- complexity: $C = \frac{\sigma_{dd\alpha}/\sigma_{d\alpha}}{\sigma_{d\alpha}/\sigma_\alpha} = \sigma_{dd}/\sigma_\alpha$

where σ_α is the standard deviation of the signal, $\sigma_{d\alpha}$ is the variance of the first derivative, and $\sigma_{dd\alpha}$ is the variance of the second derivative of the signal. Activity gives a measure of the variance of the signal. Mobility is the ratio between the standard deviation of the slope and the standard deviation of the signal σ_d/σ_α. Complexity gives a measure of excessive details with reference to the "softest" possible curve shape, the sine wave, this corresponding to unity. For our particular case, the signal window is defined by the interval $[\hat{\alpha}_{P_i} - q, \hat{\alpha}_{P_i} + q]$, where $2q$ is the size of the window centred in the ith peak or valley $\alpha(x_{P_i})$.

C. SVM Classification

Support Vector Machines are supervised learning models and are commonly used for classification analysis. A basic SVM predicts, for each given input, which of two possible classes forms the output, making it a non-probabilistic binary classifier. Given the training set, the SVM training algorithm builds a model that assigns new examples into one category or the other.

The SVM model to be trained for this work uses the RFT data and the ground truth labels to learn how to separate CF from other data (non-CF). The learned SVM model is later employed to detect CF in unseen data. CF could be further divided into B&S joints and other features, due the high presence of the former one.

Each feature descriptor $\mathbf{x}_i$ has a corresponding label y_i, where the aim of training a classifier is to learn a decision boundary from the training data pairs $(\mathbf{x}_i, y_i)$ and later use the decision boundary to predict the labels of feature vectors. The label y is broken up first into two classes CF and non-CF. As we will see later, we also consider the case of three-classes; B&S joint, other CF and non-CF.

Training a SVM model is an optimisation problem involving minimisation of (3) subject to (4) and (5) ;

$$\min \frac{1}{2} w^T w + C \sum_{i-1}^{l} \xi_i \tag{3}$$

$$y_i(w^T \phi(\mathbf{x}_i) + b) \geq 1 - \xi_i \tag{4}$$

$$\xi_i \geq 0, \tag{5}$$

where w is the normal to the hyperplane, ξ is a slack variable in case the data set is not separable, C is the cost assigned to penalise misclassification. Function ϕ is a mapping used to deal with the non-linearity of the decision function. A kernel is constructed using the dot product of the mapping function $K(\mathbf{x}_i, \mathbf{x}_j) = \phi(\mathbf{x}_i)\phi(\mathbf{x}_j)$.

The Radial Basis Function (RBF) $K = \exp(-\gamma \|\mathbf{x} - \mathbf{x}_i\|^2)$ is selected as the kernel for SVM due to its ability to deal

with non-linear relationships between the features and the corresponding labels. For our data-sets RBF kernel produced better performance than the linear and other kernels.

Training data is selected randomly from the RFT inspection data set. Each training instance $\mathbf{x}_i$ consists of the descriptor obtained from the phase and amplitude. A truth label y_i is assigned to each training instance $\mathbf{x}_i$. Firstly, the two-class problem is used to produce the SVM model. Later for the three-class problem, a multi-class model (one against all) is generated from the learning process. The model in both cases consists of the kernel parameters, the support vectors and the corresponding weights. Each feature descriptor is the Hjorth parameters of the window, magnitude of the phase and magnitude of the amplitude at feature position. The model can then be used to infer the labels $\hat{y}$ of input feature vectors, and the labels are used to identify the CF (separated either into two classes or three classes) at a given position. The output of the classifier gives the position x_{P_i} of each $\mathbf{x}_i$ classified as CF.

IV. Video Verification

A sequence of visual images of 720×576 pixels from a CCTV inspection of the empty pipeline are used to verify the findings in RFT data. The images are analysed independently to detect circle-like features, which are potential CF. A dedicated visual odometry algorithm is utilised to obtain the position of the image with respect to the RFT data.

A. CF Detector based on Delta E

In general CF such as joints, elbows or flanges are visually salient in empty pipes as high-contrast circles (see Fig. 2(b)). In this paper, we follow a similar mechanism than the proposed in [11] to detect the CF using Delta E.

The *Delta E* (ΔE) difference, where E is the German word for sensation (*Empfindung*), is used to measure the difference between colours in the CIELAB colour space. The Lab colour space [10] is composed of three components: L represents the lightness, and a and b are *colour-opponent* dimensions. These coordinates have evolved to the more recent CIE 1976 or CIELAB colour space, where the $L^*a^*b^*$ components are marked with asterisks to make a distinction between both spaces.

This colour space has many interesting characteristics when compared to the traditional RGB space. One of its most important features is that it is not dependent on the device. Another important characteristic is that it has been designed to imitate the human vision system. Since the CF are visually described based on the human perception, it appears to be an appropriate choice.

Several definitions have been proposed throughout the years to measure the ΔE difference (CIE76, CIE94, CIEDE2000, CMC l:c (1984)). In this work, the CIE76 version has been implemented for simplicity. The ΔE difference between two colours, $L_1^*a_1^*b_1^*$ and $L_2^*a_2^*b_2^*$, in the $L^*a^*b^*$ space is computed as follows,

$$\Delta E = \sqrt{(L_2^* - L_1^*)^2 + (a_2^* - a_1^*)^2 + (b_2^* - b_1^*)^2}. \qquad (6)$$

Eq. (6) is applied in our approach to extract the most significant colour transitions of an image. First, the initial image in the RGB space is converted into the CIELAB space. Next, the ΔE difference is calculated between each pixel and its neighbours. If its value is higher than a threshold, this pixel is extracted as one of the significant points of the image. This is basically a gradient-based method to detect the edges of an image, but based on ΔE differences instead of intensity changes. Different options, such as the Sobel operator or second-order methods, could also be applied to detect the colour edges. It could be possible to define an edge detector in the RGB colour space. However, this option was discarded after obtaining poorer results in some experiments.

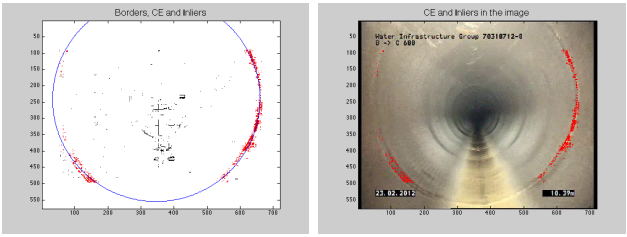

Fig. 5. ΔE-based CF detection in a frame. Left: Colour transitions (black), inliers (red), and CF (blue). Right: Image and inliers.

Once the most significant transitions have been extracted (Fig. 5 (a)), the next step consists of detecting circles in the image. From the extracted points, those of them situated close to the centre of the image are discarded because they do not belong to the CF of interest. The circle detection is based on an iterative process where the circle coordinates (centre and radius) are computed from the inliers. This is done by using the RANSAC algorithm [12].

Two conditions must be met to consider that the current frame contains a circle that corresponds to a CF: minimum number of inliers and minimum radius. The number of inliers is compared to a minimum threshold to decide if the circle is relevant enough. The second condition is related to the three-dimensional distance to the CF. The higher the radius, the closer the camera to the CF. Besides, as can be observed in the figures, the image is dark in the centre, and only circles with a minimum radius could be detected from a visual point of view.

Finally, an additional condition has been included to avoid false positives. Three consecutive frames with relevant circles must be detected to consider that a CF has been found.

To sum up, an image-based CF detector has been detailed in this section. It is composed of four steps:

1) Image conversion, from RGB to CIELAB.
2) ΔE-based colour transitions extraction.
3) Circle detection (RANSAC).
4) CF verification (minimum inliers, minimum radius and three consecutive frames with relevant circles).

B. Visual Odometry

In order to automatically verify the construction features identified by the SVM classier, it is necessary to locate the visual data in the CCTV sequence with respect to the RFT data. A dedicated visual odometry algorithm was implemented to get the location of the visual data. In this way, once a CF is detected in a given location, it can be

displayed at the specific image where it can be visually verified.

Visual odometry is the process of incrementally estimating the pose of the camera by examining the changes that motion induces on the images. An extensive survey and the principles of visual odometry can be found in [13]. In the implemented visual odometry algorithm, the image positions are estimated relative to a given starting position, based on the RFT data, by integrating incremental changes in camera pose. Our algorithm estimates the camera egomotion using sparse scene point correspondences found between consecutive frames, and their estimated position on the interior surface of the pipe in a similar way as described in [14]. Our method estimates the six degree of freedom camera poses incrementally to obtain robust estimates. The estimated position is found constraining the average of the 3D points to be inside of the nominal internal diameter of the pipe. The reference scale measurement and the nominal internal diameter provide the mechanism for removing the monocular scale ambiguity in the egomotion estimates. The algorithm uses a calibrated camera. The calibration allows to determine its intrinsic parameters, including focal length, pixel scale, and skew.

In our implementation, point features[2] are detected and tracked using the SIFT descriptor and detector [15]. Motion estimation is calculated after two frames. For initialisation, the essential matrix is estimated using the calibrated five points algorithm combined with a RANSAC algorithm [12] to solve the problem of false matches. From the essential matrix, the five degree of freedom of translation and rotation up to scale are estimated. The scale is recovered as explained above using the known internal diameter. Note that tracking more than two frames would produce more accurate results, however the type of images obtained from inside the pipes produce sparse matches that do not allow to track interest point for long periods.

C. Automatic Verification

The verification is performed automatically once the CF has been identified in the RFT data and a circle-like feature has been detected in the visual images at the same location. As mentioned above, the image location with respect to the RFT inspection is produced by the visual odometry algorithm.

V. Experimental Results

Two sources of multi-modal data are used in this work to evaluate and validate our approach, the data from the RFT tool of Fig. 1(a) and a CCTV inspection of the same pipeline. The section inspected is a cement-lined cast-iron pipe part of a water distribution network of 983m length[3]. The CCTV footage and RFT data are not synchronised as they were taken in two separate runs; 1) the See-Snake tool submerged in water and 2) a mobile robot with a single camera driving in the empty pipeline (for visibility purposes). The initial frame with respect to the RFT data was located manually.

A. Evaluation of the Classifier

In order to learn the model and assess the performance of the classifier, we have labeled all the construction features manually using both RFT and CCTV data. A total of 228 CF were found in the 783m of data, where 207 are B&S joints and the rest are either elbows or flanges.

LibSVM [16] is used for the implementation of the classifier. In order to optimise the SVM performance, a grid-search of the optimal parameters over the RBF kernel was performed. The two parameters used in RBF kernel are γ and C in 3. C is the cost assigned to penalise misclassification. Lower cost results in soft margin which results in high classification errors whereas higher cost generates a more accurate model but may lead to over-fitting. γ is the width of RBF which determines the smoothness of the model.

For the two classes $\{CF, Non-CF\}$ problem, cross validation was used to test the model learned from the data and prevent over fitting. A 10-fold cross validation produced the results presented in Table I. The feature extraction algorithm obtained a total of 3055 features along the 783m. These features correspond to all the instances of the data set. Fig. 6(a) presents the detection and identification results between 330m and 460m using the best trained model.

Table I shows quantitative results comparing the proposed descriptor with a simple descriptor consisting of the straightforward choice of the normalised sum of the phase and the amplitude at the peaks location. Note that due to the high number of Non-CF features in the data set ($2830/3055$), the resulting accuracy will always be high, *i.e* even if all CF are misclassified the accuracy will be 92.6%. Thus, more interesting parameters to look at are the precision and recall of the CF class and the overall confusion matrix. As the table shows, the proposed descriptor reduces the number of false positives and more importantly false negatives, which are the actual CF that were not classified as CF increasing the recall and precision.

Moreover, the generalisation of the algorithm in CF detection was tested using unseen data (first 100m of the inspection) retained by Russell NDE Systems Inc. The proposed algorithm produced 100% correct detection of all CF.

As mentioned above, we also extended the classification problem into a three-class one, where the aim was to differentiate B&S joints from other CF. In this case, three classes are considered $\{B\&S, CF, non-CF\}$. Due to the low quantity of the CF class, it is not feasible to do a proper n-fold cross-validation so we opted to show the results only on training using the full data set. Table II summarises the results obtained from the training data and compares it with the simple descriptor. Fig. 6(b) shows the detection and identification results between 330m and 460m. This results show again our proposed descriptor outperforms the simple descriptor in particular for the case of other CF, where very few examples are given.

[2]Note that these point features are different from the circle-like features obtained to detect potential CF.

[3]The first and last 100m of the inspection were held back at Russell NDE Systems for internal evaluation.

TABLE I

COMPARISON USING CONFUSION MATRIX, PRECISION, RECALL AND ACCURACY FOR SVM CLASSIFICATION RESULTS FOR 10-FOLD CROSS-VALIDATION OF THE TWO-CLASS PROBLEM WITH THE PROPOSED DESCRIPTOR AND THE SIMPLE DESCRIPTOR.

	Proposed descriptor			Only $\mathbf{x} = [\hat{\alpha}(x_P), \hat{a}(x_P)]$		
	$\widehat{CF}$	$\widehat{Non-CF}$	Recall (%)	$\widehat{CF}$	$\widehat{Non-CF}$	Recall (%)
CF	20 ± 5	3 ± 1	$\mathbf{89.9 \pm 3.2}$	17.5 ± 5	5 ± 1	$\mathbf{76.6 \pm 6.8}$
$Non-CF$	2 ± 1	280 ± 13	$\mathbf{99.0 \pm 0.3}$	3 ± 1	280 ± 9	$\mathbf{99.0 \pm 3.8}$
Precision (%)	$\mathbf{87.8 \pm 4.6}$	$\mathbf{99.2 \pm 0.3}$		$\mathbf{86.1 \pm 5.8}$	$\mathbf{98.2 \pm 0.4}$	
Accuracy (%)	98.34 ± 0.9			97.45 ± 0.4		

TABLE II

COMPARISON USING CONFUSION MATRIX, PRECISION, RECALL AND ACCURACY FOR SVM CLASSIFICATION RESULTS FOR THE THREE-CLASS PROBLEM WITH THE PROPOSED DESCRIPTOR AND THE SIMPLE DESCRIPTOR.

	Proposed descriptor				Only $\mathbf{x} = [\hat{\alpha}(x_P), \hat{a}(x_P)]$			
	$\widehat{B\&S}$	$\widehat{CF}$	$\widehat{Non-CF}$	Recall (%)	$\widehat{B\&S}$	$\widehat{CF}$	$\widehat{Non-CF}$	Recall (%)
$B\&S$	201	0	0	**100**	188	0	13	**93.5**
CF	0	24	0	**100**	2	10	12	**41.6**
$Non-CF$	4	0	2826	**99.86**	26	0	2804	**99.1**
Precision (%)	**98.0**	**100**	**100**		**87.3**	**100**	**99.11**	
Accuracy (%)	99.87				98.26			

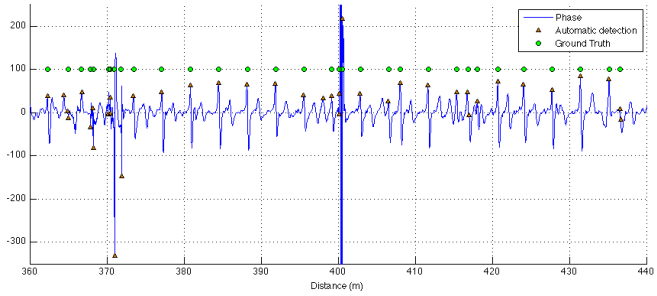

(a) two-class SVM

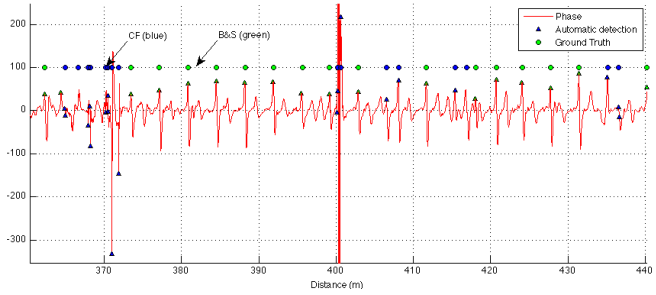

(b) three-class SVM

Fig. 6. Classification of construction features produced by the two and three-class SVM. The classified CF are shown as triangles and the ground-truth is shown as circles. Note that is the result of the classification of the detected features shown in Fig. 4 for the interval from 360 to 440m.

B. Video Verification Validation

The best SVM model obtained in the 10-fold cross validation for two classes and the SVM model for three classes were used to detect the CF in the whole data set (783m), as shown in Figures 6(a) and 6(b) for the $\sim$ 80m section. The locations of the features classified as CF were associated with the CCTV using the visual odometry algorithm described in Section IV-B. The nominal internal diameter of the pipe is 590mm. This quantity is used to compute automatically the scale in the single camera visual odometry algorithm. Vedaldi's SIFT implementation [17] was used in this work. Fig. 7 shows an example of the images matches and the trajectory of the mobile robot's camera of the CCTV inspection.

The configuration parameters to detect circle-like features in the images are; the minimum radius equals to 100 pixels (equivalent to a distance from the camera of 0.8m), 400 as the minimum number of inliers, 20 pixels as the acceptance distance to consider a point as an inlier and ΔE threshold to extract a significant point equal to 5. The proposed method is able to efficiently detect potential CF using the information provided by the camera as shown in Figures 8 and 9 and in the video attached. Note that the circle-like features are necessarily CF, but all CF are seen in the images as circles.

In order to show graphically the results of the detection, identification and verification, a simple visual interface has been implemented (see video attached). The visual interface displays the matches in two consecutive images at 5 frames per second. The identified CF is displayed when it is located between 0.6 and 1.4m in front of the camera to account for odometry errors. Once both multi-modal sources agree a message prompt is displayed to the user as the CF is verified in a given axial position.

Figures 8 and 9 show in the visual image examples of verified CF. The horizontal line with a position is the result of the classification algorithm on the RFT data, while the red points are the inliers of the circle-like features detected in the image.

Fig. 8 presents multiple frames where B&S joints are identified using the SVM model for three classes, detected by Delta E algorithm and associated in location using the visual odometry algorithm. In the other hand, Fig. 9 shows other CF found in the data set such as an elbow and an unknown feature also using the model for three classes. Note that only few examples of this class were available on the data, however our classifier was still able to discriminate them as shown in Table II.

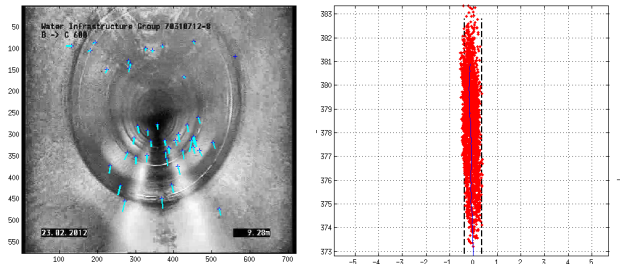

(a) Image and Features (b) Path and 3D points

Fig. 7. Visual odometry results for 100 m. The left plot shows the SIFT feature matches in consecutive frames. The right plot show top view of the camera trajectory with points within the nominal pipe diameter.

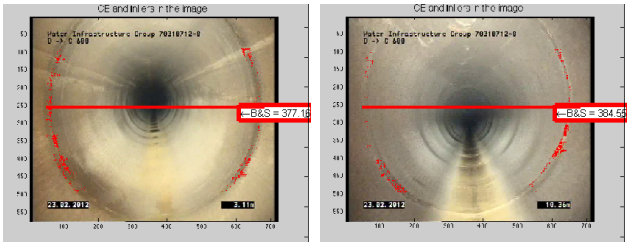

(a) Frame 410 at 377.16m (b) Frame 628 at 384.55m

Fig. 8. B& S joints displayed onto the corresponding visual images after detection in RFT data.

VI. Conclusions

This paper proposes an automatic approach to detect, identify and verify construction features using multiple sensing modalities such as RFT signals and visual images. The introduced approach identifies construction features in RFT data and displays them in visual images. The construction features' identification using RFT signals has been addressed by developing a new descriptor for a SVM classifier. Quantitative results showed our descriptor reduces significantly the number of false positives, but more importantly, false negatives. RFT and visual images data are associated through position using a dedicated visual odometry algorithm.

We also proposed a circle-like feature detection algorithm on visual images. This detector allows the verification step to be fully automated. Once the CF have been identified and circle-like features are detected at the same location, the CF are verified. This approach aims to help condition assessment analysts to locate correctly pipe sections that are between joints, flanges and elbows.

ACKNOWLEDGMENT

This publication is an outcome from the Critical Pipes Project funded by Sydney Water Corporation, Water Research Foundation of the USA, Melbourne Water, Water Corporation (WA), UK Water Industry Research Ltd, South Australia Water Corporation, South East Water, Hunter Water Corporation, City West Water, Monash University, University of Technology Sydney and University of Newcastle. The research partners are Monash University (lead), University of Technology Sydney and University of Newcastle.

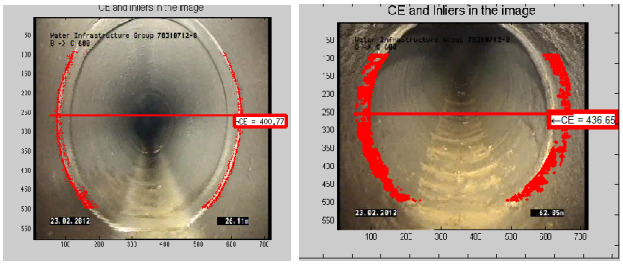

(a) Frame 1093 at 400.23m (b) Frame 3940 at 436.65m

Fig. 9. Other construction features displayed onto the corresponding visual images after detection in RFT data. a) Unknown feature, and b) elbow.

References

[1] M. Bracken and D. Johnston, "Acoustic methods for determining remaining pipe wall thickness in asbestos cement, and ferrous pipes," in *Procs of Pipelines 2009: Infrastructure's Hidden Assets.*, 2009, pp. 271–281.

[2] C. Edwards and S. B. Palmer, "The magnetic leakage field of surface-breaking cracks," *Journal of Physics D: Applied Physics*, vol. 19, no. 4, p. 657, 1986.

[3] D. Atherton, "Remote field eddy current inspection," *IEEE Transactions on Magnetics*, vol. 31, no. 6, pp. 4142–4147, 1995.

[4] C. J. C. Burges, "A tutorial on support vector machines for pattern recognition," *Data Mining and Knowledge Discovery*, vol. 2, pp. 121–167, 1998.

[5] B. O. Hjorth, "Technical contributions eeg analysis based on time domain properties," *Electroncephalography and Clinical Neurophysiology*, vol. 29, pp. 306–310, 1970.

[6] A. Khodayari-Rostamabad, J. Reilly, N. Nikolova, J. Hare, and S. Pasha, "Machine learning techniques for the analysis of magnetic flux leakage images in pipeline inspection," *IEEE Transactions on Magnetics*, vol. 45, no. 8, pp. 3073–3084, 2009.

[7] B. Wijerathna, T. Vidal-Calleja, S. Kodagoda, Q. Zhang, and J. Valls Miro, "Multiple defect interpretation based on gaussian processes for mfl technology," *Proc. SPIE Nondestructive*, vol. 8694, pp. 86 941Z–86 941Z–12, 2013.

[8] M. Davoust, L. Le Brusquet, and G. Fleury, "Robust estimation of hidden corrosion parameters using an eddy current technique," *Journal of Nondestructive Evaluation*, vol. 29, no. 3, pp. 155–167, 2010.

[9] S. Hensel, C. Hasberg, and C. Stiller, "Probabilistic rail vehicle localization with eddy current sensors in topological maps," *IEEE Transactions on Intelligent Transportation Systems*, vol. 12, no. 4, pp. 1525–1536, 2011.

[10] R. S. Hunter, "Photoelectric color-difference meter," in *Proceedings of the Winter Meeting of the Optical Society of America*, 1948.

[11] F. Martín, J. Valls Miró, and L. Moreno, "Towards exploiting the advantages of colour in scan matching," in *ROBOT2013: First Iberian Robotics Conference*, ser. Advances in Intelligent Systems and Computing, M. A. Armada, A. Sanfeliu, and M. Ferre, Eds. Springer International Publishing, 2014, vol. 253, pp. 217–231.

[12] M. A. Fischler and R. C. Bolles, "Random sample consensus: A paradigm for model fitting with applications to image analysis and automated cartography," *Commun. ACM*, vol. 24, no. 6, pp. 381–395, June 1981.

[13] D. Scaramuzza and F. Fraundorfer, "Visual odometry [tutorial]," *IEEE Robot. Automat. Mag.*, vol. 18, no. 4, pp. 80–92, 2011.

[14] P. Hansen, H. Alismail, P. Rander, and B. Browning, "Monocular visual odometry for robot localization in lng pipes," in *Robotics and Automation (ICRA), 2011 IEEE International Conference on*, 2011, pp. 3111–3116.

[15] D. G. Lowe, "Distinctive image features from scale-invariant keypoints," *International Journal of Computer Vision*, vol. 60, pp. 91–110, 2004.

[16] C.-C. Chang and C.-J. Lin, "LIBSVM: A library for support vector machines," *ACM Transactions on Intelligent Systems and Technology*, vol. 2, pp. 27:1–27:27, 2011, software available at http://www.csie.ntu.edu.tw/ cjlin/libsvm.

[17] A. Vedaldi and B. Fulkerson, "VLFeat: An open and portable library of computer vision algorithms," 2008, software available at http://www.vlfeat.org/.